Advanced Radar Geosynchronous Observation System: ARGOS

Andrea Monti Guarnieri, *Member, IEEE*, Antoni Broquetas, Andrea Recchia, Fabio Rocca, and Josep Ruiz-Rodon

***Abstract*—The Advanced Radar Geosynchronous Observation System is proposed to be a multiple-input–multiple-output synthetic aperture radar (SAR) system hosted on a swarm of minisatellites in quasi-geostationary orbits. The system is made of N iso-frequency sensors, each of them transmitting and receiving the signals. The system would combine the continuous imaging capabilities of a geostationary SAR, gaining a factor N^2 in signal-to-noise ratio (SNR). The real aperture would be achievable in $\sim$40 min, enabling applications so far unseen, such as monitoring fast deformations, landslides, and other applications for emergency and security. Still, the SNR of the long acquisition time would be conserved. The optimal design of the swarm is addressed, in order to trade resolution, coverage, and revisit time.**

***Index Terms*—Earth Observing System, multiple-input–multiple-output (MIMO) radar, radar interferometry, spaceborne radar, synthetic aperture radar (SAR).**

I. Introduction

GEOSYNCHRONOUS synthetic aperture radar (SAR) exploits orbit eccentricity and inclination to get a suitable synthetic aperture, whereas the strong path loss attenuation is compensated by means of both medium- and long-term integration times, large transmitted power, and large antenna reflectors. Two concepts have so far been proposed: the geosynchronous and the quasi-geostationary SAR. The *geosynchronous* SAR, which is shown in Fig. 1 (top), which was first proposed in [1], achieves a continental coverage and one-day revisit by exploiting significant orbit inclination and eccentricity. Spread losses are compensated by huge antenna and high power, which would require 2020 technologies [2]. It is obtaining growing interest in recent literature [3]–[5].

The *geostationary* SAR with regional coverage is represented in Fig. 1 (bottom) in the original bistatic configuration [7]. The system compensates spread losses by long integration times (hours) and therefore exploits moderate power and medium-size antennas. It is then suited to be embarked as a monostatic payload of opportunity on a communication satellite (COMSAT) [7]. In that case, the maximum allowed orbit jitter of $\pm 0.1^\circ$ would leave a synthetic aperture of 150 km, which, in turn, allows generating SAR images in a continuous tradeoff between observation and resolution that scales from $\sim$100 m in 20 min to 5 m in 8 h in X-band. Such quasi-continuous imaging capability is a unique feature of geostationary SAR, which enables a wide variety of applications, some unprecedented, such as the estimation of water vapor maps at fine resolution on land for Numerical Weather Prediction, detecting precursors for landslides or eruption hazards monitoring (see [8] for an overview).

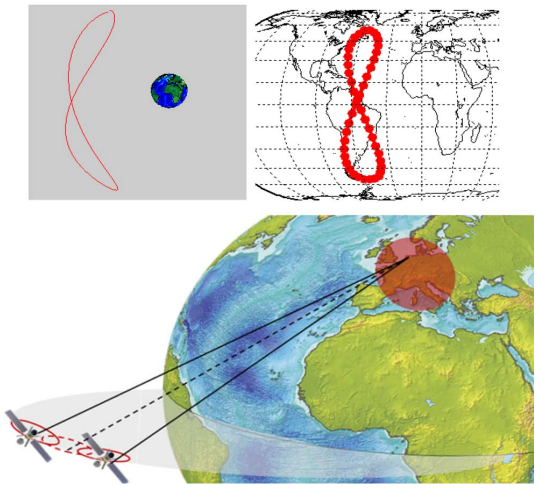

Fig. 1. (Top) Orbit (in scale) and nadir track of a typical geosynchronous SAR with continental coverage, characterized by a significant inclination and eccentricity. (Bottom) Representation of a bistatic quasi-geostationary SAR with regional coverage, whose orbit has near-zero inclination and small eccentricity. The dotted lines refer to its monostatic equivalent.

Nonetheless, geostationary SAR image quality is impaired by both the atmospheric phase screen (APS) [3], [9]–[11] and the backscatter decorrelation in the one-day revisit. The mitigation of decorrelation demands for long wavelengths, and in fact, typically, L-band is proposed for geosynchronous SAR. However, this choice limits the achievable azimuth resolution to, for example, 1.3 km, single look, after 20 min of synthetic aperture, down to 40 m in 7–8 h. This reduces the observation capabilities and the applications to wide-scale monitoring.

In this letter, we propose a different concept, which is named ARGOS, from the mythological 100-eyed giant, that is an enhancement of the geostationary SAR. The Advanced Radar Geosynchronous Observation System (ARGOS) bases on a swarm of N iso-frequency minisatellites in closed flight

Manuscript received November 11, 2014; revised January 13, 2015, February 9, 2015, and February 11, 2015; accepted February 12, 2015. Date of publication March 5, 2015; date of current version March 24, 2015.

A. Monti Guarnieri, A. Recchia, and F. Rocca are with the Dipartimento di Elettronica, Informazione e Bioingegneria, Politecnico di Milano, 20133 Milano, Italy.

A. Broquetas and J. Ruiz-Rodon are with the Signal Theory and Communications (TSC) Department, Universitat Politecnica de Catalunya, 08034 Barcelona, Spain.

Color versions of one or more of the figures in this paper are available online at http://ieeexplore.ieee.org.

Digital Object Identifier 10.1109/LGRS.2015.2404214

formation [12], a multiple-input–multiple-output (MIMO) SAR [13], [14] with $N_{\mathrm{TOT}} = N \times (N+1)/2$ center of phases that are displaced along longitudes to sample the synthetic aperture. In the following, we assume $N = 6$ as this is the number of minisatellites of less than 300-kg payload, which could be launched simultaneously by an Ariane 5 class launcher. The formation, by tessellating and parallelizing the scan of the Doppler frequencies axis, allows generating a new image in about 40 min, while maintaining the SNR correspondent to the long acquisition time with a single satellite. Being free from clutter and atmospheric artifacts, the system could benefit from the large bandwidths and the small antennas typical of X-band. Furthermore, the freedom degrees in tuning the orbit parameters give space to different configurations of the swarm, where resolution can be traded in flight for coverage, or revisit time.

II. Monostatic Geostationary SAR: Design and Performances

Each single monostatic satellite's orbit around a fixed reference on Earth can be described in polar coordinates [15], i.e.,

$$\begin{aligned} r(t) &= R_{\mathrm{geo}}\left(1 - e_n \cos\left(\Omega_E\left(t - t_n\right)\right)\right) \\ \psi(t) &= \psi_n + 2e_n \sin\left(\Omega_E\left(t - t_n\right)\right) \end{aligned} \tag{1}$$

where $R_{\mathrm{geo}} = 42\,164.2$ km is the average geosynchronous orbit radius, $\Omega_E = 2\pi/86\,400$ is the Earth angular speed, $r(t)$ is the instantaneous orbit radius, and $\psi(t)$ is the instantaneous longitude. The orbits in (1) describe small ellipses, such as those shown in Fig. 1, centered at latitude ψ_n and with eccentricity e_n. The parameter t_n is the reference time chosen as the satellites cross over the perigee. In (1), zero orbit inclination is assumed to avoid baseline decorrelation [7], as this is not relevant for the synthetic aperture, although a slight inclination could be introduced for a safe constellation keeping [17]. We have also ignored a longitude drift [12], indeed quite small. The small baselines considered limit cross-track resolution and then tomographical applications, which need a different L-band constellation [16].

The orbit of each satellite in the swarm is then fully described by the tern of parameters $\{\psi_n, e_n, t_n\}$. The eccentricity plays a fundamental role, as it fixes the along-track angle span, i.e., $\Delta\Psi_{\mathrm{n}} = 4e_n$; therefore, the synthetic aperture, i.e., L_{sn}, and the resolution, i.e., ρ_{azn}, of each monostatic system are

$$L_{\mathrm{sn}} = 4R_{\mathrm{geo}}e_n \qquad \rho_{\mathrm{azn}} = \frac{\lambda}{2L_{\mathrm{sn}}}R = \frac{\lambda R}{8R_{\mathrm{geo}}e_n} \tag{2}$$

where λ is the wavelength, and R is the satellite–target distance $\sim$38 000 km at 45° latitude. Notice that the variation of the orbit radius, i.e., R in (1), is irrelevant as for the synthetic aperture. The azimuth resolution in (2) can be made pretty good, $\sim$5 m, by assuming X-band and the maximum eccentricity allowed for a COMSAT, i.e., $e \sim 8 \cdot 10^{-4}$. Achieving that resolution would not be simple, since the design of the monostatic system is constrained by the severe path loss and then by SNR [6], [7], i.e.,

TABLE I
Geostationary Monostatic SAR Design, X-Band

Parameter	Unit	Value		
		Near Range	Mid Range	Far range
Polarization			HH	
Ground Range resolution	m	21	20	19
Azimuth resolution:				
coarse (40 min)	m		54	
fine (12 hour)	m		5	
Mean power	W		150	
Antenna Directivity	dB	49.5	52.5	49.5
Antenna Eq. Area	dBsm	8.38	11.4	8.38
EIRP	$\mathrm{dB_W}$		19.0	
Path losses	dB	-162.6	-162.6	-162.7
Total losses	dB		-4.0	
Target backscatter	dBsm	-11	-11.6	-11.8
Noise spectrum density	$\mathrm{dB_W}$		-202	
NESZ	dB	-16.1	-21.2	-16
SNR	dB	4.8	9.6	4.2

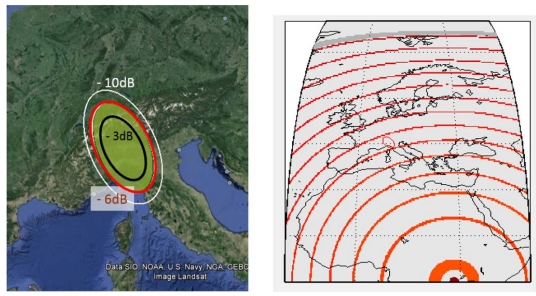

Fig. 2. X-band monostatic geostationary SAR. (Left) Antenna footprint, 250 × 430 km at −6 dB. (Right) Dartboard diagram [7] for PRF = 340 Hz, 10% duty cycle.

$$\mathrm{SNR} = \frac{P_t G A \eta_T}{(4\pi R^2)^2}\frac{\sigma^0 \rho_{\mathrm{az}}\rho_{\mathrm{rg}}}{\sin\theta}\frac{T_S}{N_0} = \frac{P_t G A \eta_T}{(4\pi)^2 R^3}\frac{\sigma^0 \rho_{\mathrm{rg}}\lambda}{2v_s \sin\theta}\frac{1}{N_0} \tag{3}$$

where P_t is the mean transmitted power; G and A are the antenna gain and area, respectively; η are the total losses; σ^0 is the backscatter coefficient; θ is the incidence angle; ρ_{az}, ρ_{rg} are the azimuth and range resolutions, respectively; N_0 is the noise power spectrum; T_s is the synthetic aperture time; and v_s is the mean velocity in the useful aperture interval. The rightmost expression, which is derived by exploiting (2), shows that SNR is independent of the observation time, for the distributed target case, since the synthetic aperture time and the azimuth resolution are inversely proportional.

Performances are summarized in Table I for the X-band system located at 28° longitude shown in Fig. 2 and referred to an image resolution of 20 × 20 m, 4 looks. The SNR is 4 dB at the swath edges for an average transmitted power $P_t = 150$ W.

The quick-look azimuth resolution, for example, in 40-min aperture, is pretty coarse even in X-band, 50 m, whereas the swath width is actually constrained by the limited power. Furthermore, data quality is impaired by the decorrelation that occurs in the one-day interferometric revisit and from tropospheric turbulence.

Examples of correlation matrixes acquired in different scenes of grass and short vegetation and different seasons, using a

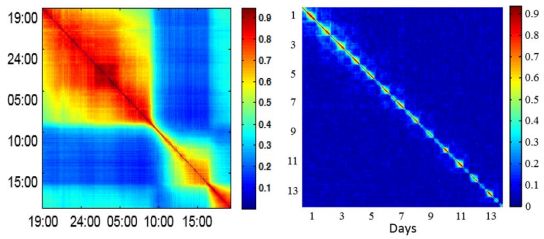

Fig. 3. Examples of Ku-band correlation matrixes over grass fields, from different ground-based SAR acquisitions. (Left) One day, area of Berne (CH), spring. (Right) Twelve days, area of Beauregard (Italy), summer.

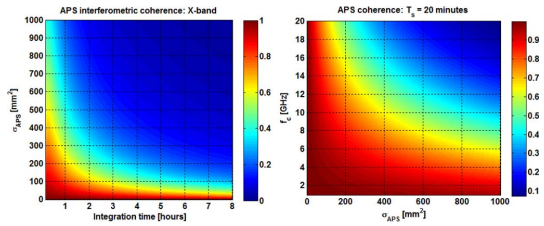

Fig. 4. Decorrelation due to the uncompensated APS computed according to [15]. (Left) X-band case and function of $\sigma_{\rm APS}$ and integration time. (Right) Twenty-minute integration time and function of $\sigma_{\rm APS}$ and frequency.

Ku-band ground-based SAR [9], are shown in Fig. 3. Coherence is lost from day to day, as well as during the day within hours. This prevents any interferometric applications unless relying on persistent scatterers, [16], which give limited results at such coarse resolution.

On top of this, the APS adds further decorrelation, in the long integration time (minutes), which can be so strong to demand for L-band as a safe choice [3], [4], [10]. The APS decorrelation shown in Fig. 4 has been computed according to [11] and by assuming a space–time APS variogram (which is the standard deviation of the differential delay measured in two targets and distance r meters, after t seconds), i.e.,

$$\sigma^2_{\rm APS}(t,x) = 2\sigma^2_{\rm APS}\left(\sqrt{\left(\frac{t}{t_0}\right)^2+\left(\frac{r}{r_0}\right)^2}\right) \tag{4}$$

where the APS time and space constants were assumed $t_0 = 10$ h and $r_0 = 20$ km. It appears from Fig. 4 that practical values of $\sigma^2_{\rm APS}$ in the range 400–800 mm^2 lead to significant "clutter" for images taken in X-band during an aperture of, for example, 1 h, whereby an aperture of 20 min would quite get a moderate clutter at all frequencies up to Ku-band.

III. Geostationary Swarms

The combination of two satellites, each transmitting and receiving, results in three phase centers, the third one spanning the equivalent elliptical orbit shown in Fig. 1. In the case of $N = 6$ geosynchronous minisatellites so far discussed, an ideal uniform distribution of the $N_{\rm TOT} = 21$ phase centers, as many as the combination with repetition, would get a full real aperture in 12 h/21–35 min. This is the overall fine-resolution image time, whereas the interferogram revisit would be in the average half of that, i.e., 20 min. In such time, the impact of scene decorrelation [6], which is also known in lunar SAR papers [18], [19], and APS will be decriticized, as shown in Figs. 3 and 4.

A. Link Budget

In order to evaluate the *link budget*, the intuitive way is to say that we have six transmitters and six receivers; thus, the total power is six times; the same goes for the receiving area; thus, in total, we achieve a gain of 36 with respect to the monostatic case.

Another way to arrive at the same result, which may be more acceptable, is the following. Let us consider any monostatic or bistatic couple. In the real aperture time, for example, 40 min, each couple operates on an azimuth resolution that is approximately 1/21 of the total. Combining the different monostatic/bistatic systems, we achieve full azimuth resolution indeed, but the SNR is the one calculated with the low resolution. This gives us a factor $N_{\rm TOT} = 21$. Then, we have to consider the double takes, namely, when satellite A is transmitting and satellite B is receiving and vice versa, while they are illuminating the very same wavenumber. Here, we have to sum the two energies: in total, we have that the factor 21 has to be augmented by the probability of each wavenumber being covered twice and therefore has to be multiplied times the factor $f = \{1 + 15/21\}$. In conclusion, $21 \cdot f = 36$ or $N \times (N+1)/2 + N \times (N-1)/2 = N^2$.

Now, if we integrate the return signal in this time interval, we get the link budget as from (3), i.e.,

$$\text{SNR} = 6 \times 6 \frac{P_t G A \eta_T}{(4\pi)^2 R^3} \frac{\sigma^0 \rho_{\rm rg} \lambda}{2 v_s \sin\theta} \frac{1}{N_0}. \tag{5}$$

In this case, the observation time, therefore, will be taken to be about 2400 s, as the real antenna is not fully sampled before that time. The gain by a factor 36 can be traded to achieve fine resolution while keeping constant SNR in (3): the 54×20 m resolution cell achieved after 40 min in the monostatic configuration in Table I would correspond to $54 \times 20/36 \sim 5.4 \times 5.4$ m in MIMO. Then, after 40 min, the antennas either could be steered toward a different target or could stay, improving stable targets imaging.

IV. ARGOS Configurations

The eccentricities, the ascending node times, and the center longitudes are free parameters that can be tuned to configure and reconfigure the constellation according to applications. Here, we propose two different configurations, which are represented in Fig. 5. In the *iso-elliptical* configuration, all the satellites move synchronously with respect to fixed Earth, which is with the same eccentricity vectors

$$\mathbf{E}_n = e_0 \exp\left(j\Omega_E t_0\right). \tag{6}$$

The orbits in (1) just differs by the central longitudes, i.e., ψ_n, to be optimized for all the satellites but the two extreme. In the *concentric* configuration, all the satellites share the same longitude, but with different eccentricity vectors to be optimized.

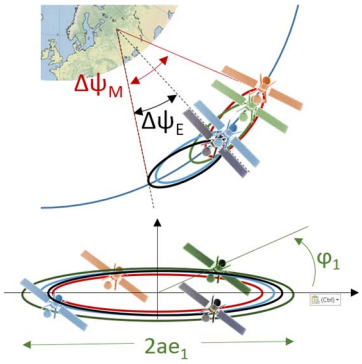

Fig. 5. Swarm configurations. (Top) Iso-elliptical. (Bottom) Concentric.

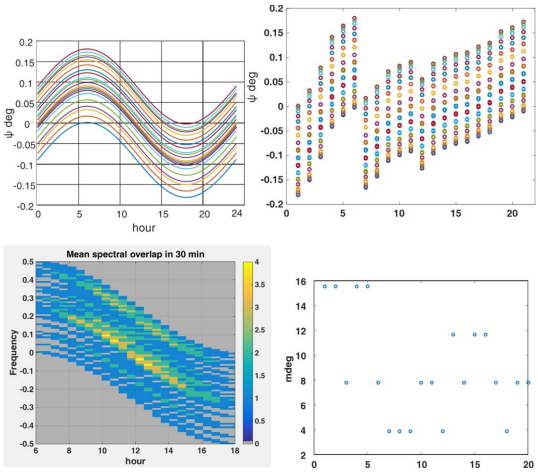

Fig. 6. Iso-elliptical optimized swarm. (Top left) Angles spanned by each phase center as a function of time. (Top right) Superposition of all the angles, the first six columns corresponding to the satellites orbits, the others to the equivalent monostatic. (Bottom) Spectral overlaps in 30′ and angles differences.

A. *Iso-Elliptical Swarm*

In the iso-elliptical swarm, which is shown in the upper graph in Fig. 5, the orbits share the same eccentricity vectors; therefore, the freedom degrees are the $N-2$ central longitudes ψ_n $(n=2,\ldots,N-1)$; the absolute eccentricity is e_0; the overall span of the constellation is $\Delta\psi_M$ shown in the figure.

The idea in this configuration is to keep fixed the angular shift of the satellites with time. The result after optimization on the four central longitudes is the one shown in Fig. 6: the instantaneous angles of all the 36 phase centers, proportional to the Doppler, are in the top left plot. At each time, the total angular aperture spanned, i.e., $\Delta\psi_M$, gives an image resolution (2), i.e.,

$$\rho_{\text{az}} = \frac{\lambda}{2R_{\text{geo}}\Delta\psi_M}R. \tag{7}$$

The mean angle sweeps as a sinus with time, leading in 24 h to a total "extra fine resolution," i.e.,

$$\rho_{\text{az\_24}} = \frac{\lambda}{2R_{\text{geo}}\left(\Delta\psi_M+\Delta\psi_E\right)}R. \tag{8}$$

When $\Delta\psi_M$ gets larger than $\Delta\psi_E$, resolution gets coarse, but image time and revisit reduce. In the example shown in the figure, $\Delta\psi_E$ has been equated to $\Delta\psi_M$.

The optimization has been run with the goal of minimizing the difference between the maximum and minimum distances of phase centers (that stay fixed with time), i.e.,

$$g = \max\left(\psi_n-\psi_m\right)-\min\left(\psi_n-\psi_m\right) \tag{9}$$

and adding a penalty to avoid coincident phase centers. This difference is shown in the bottom right plot in the figure.

In order to assess the effective image time, histograms of angles spanned in 30-min intervals have been computed all along half an orbit, as shown in the bottom left panel in Fig. 6. The spectral coverage is better than 80% for 75% of the time. It would be interesting to achieve the best coverage at dawn and early morning, where best performances are expected due to both scene coherence (see Fig. 3) and calm APS [9].

1) Separation in the Doppler Domain: At a first glance, one would think that the duty cycle is to be made N times smaller, as all the satellites have to be enabled to transmit, in turn. However, this drawback could be avoided by letting all SAR transmitting simultaneously and then separating the different contributions in the Doppler domain. We could do it if the Doppler bandwidth B_R, which is spanned during the real aperture time, i.e., T_R, is much smaller than the instantaneous Doppler shift between two closest equivalent monostatic phase centers B_M, i.e.,

$$B_D = \frac{2v_s}{\lambda}\frac{\lambda}{v_sT_R} \ll B_m = \frac{2v_s}{\lambda}\frac{\Delta\psi_M}{21}. \tag{10}$$

Then, by combining with (7)

$$\frac{1}{T_R} \ll \frac{v_s}{\lambda}\frac{\lambda R}{21\cdot 2\rho_{\text{az}}R_{\text{geo}}} \approx \frac{v_s}{42\cdot\rho_{\text{az}}} \Rightarrow T_R \gg \frac{42}{v_s}\rho_{\text{az}}.$$

That is satisfied with good margin if we consider a resolution in the order of few meters and a real aperture time of tens of minutes, as well as a typical value $v_s\sim 5$ m/s.

B. *Concentric Swarm*

The nonuniform spectral coverage with time can be avoided by the dual configuration, the concentric swarm, achieved by assuming all sensor's orbits concentric and tuning the eccentricity vectors, as shown in Fig. 5, in a carthwheel-like configuration [12]. In this case, the optimization has been carried out by maximizing the spectral coverage, for example, by minimizing the number of spectral holes shown in the bottom left plot in Fig. 7.

Notice that the coverage is random, but the result is uniform all over orbit time. The eccentricity of the satellites orbits, which are marked by "×" in the bottom right plot, are almost constant in amplitudes, whereas their phases are unevenly spaced, to avoid concentrations close to the origin of the equivalent monostatic orbits eccentricity. This means that we could just optimize the $N-1$ arguments of eccentricity, getting a dual design with respect to the iso-elliptical configuration. The spectral coverage, which is shown in Fig. 8 (right), is better than 80%. Spectral holes can be handled by interpolating the 12-h observations.

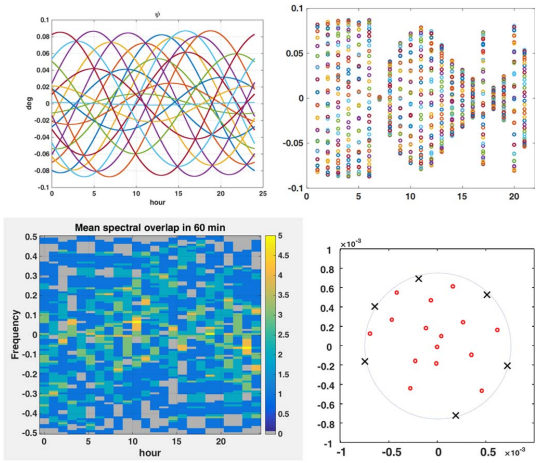

Fig. 7. Concentric optimized swarm. The (top left) spanned angles with time and (top right) angles are the same as for Fig. 6. The (bottom left) histograms of spectral overlaps are here measured over 60′ intervals. (Bottom right) ("×") Eccentricity vectors of the satellites and the ("o") monostatic equivalents.

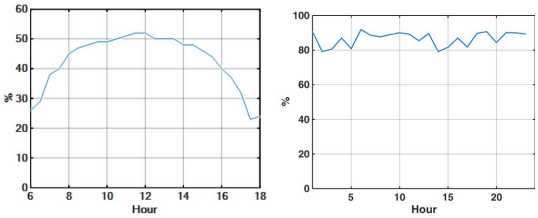

Fig. 8. Percentage of spectral coverage in (left) 30′ for iso-elliptical configuration and (right) 60′ for concentric configuration.

TABLE II
COMPARISON BETWEEN GEOSYNCHRONOUS AND LEO SAR CONCEPTS

	GEO SYNCHRONOUS	GEO STATIONARY		LEO
		MONOSTATIC	SWARM	
Coverage	Continental	Regional (limited by SNR)	Regional	World
Orbit	Significant inclination	Δlong<±0.1° Small eccentricity		
Image time	Minute(s)	20 min: quick look 7 hr: full res.	**40 minutes: full resolution**	< 1 sec
APS	Almost Frozen	Sensed - To be compensated	**Sensed and compensated**	Frozen
Line Of Sight	East-West	North-South	North-South	East-West
Revisit time	Once a day	Twice a day	**40 minutes**	Days
System	Dedicated sensor, 2020+ technologies	Payload on a GEO COMSAT	Swarm of mini satellites	Dedicated satellite

V. CONCLUSION

We have introduced a new geosynchronous SAR concept that is based on an iso-frequency swarm of minisatellites. A comparison between this and other spaceborne SARs is given in Table II. The system gets several advantages with respect to a single geosynchronous SAR.

A fine-resolution image is achieved in a much shorter time, for example, 30′ in place of 8 h, and the resolution is decoupled from the wavelength, leaving space for application-based optimizations. Moreover, having completed an image in 30′, we are able to reconfigure the sensor's operative modes, i.e., achieving a different tradeoff between coverage and resolution. A second set of advantages of the swarm stays in the fact that the global receiving antenna is six times larger than in the monostatic case and the transmitting power is six times larger for the multiplicity of the transmitters. Thus, the overall size approaches that of the high-inclination case (Tomiyasu's figure of 8, in Fig. 1). The N^2 gain in SNR can be then exploited to shorten the image time and shrink the resolution cell.

A final advantage is the graceful degradation in the case of single failures. The receivers of possible spares could be operative, adding N phase centers for each spare. The link budget would also improve with the receiving antennas.

REFERENCES

[1] K. Tomiyasu, "Synthetic aperture radar in geosynchronous orbit," in *Proc. Antennas Propag. Soc. Int. Symp.*, May 1978, vol. 16, pp. 42–45.
[2] S. N. Madsen, C. Chen, and W. Edelstein, "Radar options for global earthquake monitoring," in *Proc. IGARSS*, 2002, vol. 3, pp. 1483–1485.
[3] L. Kou, M. Xiang, X. Wang, and M. Zhu, "Tropospheric effects on L-band geosynchronous circular SAR imaging," *Radar, Sonar & Navigat., IET*, vol. 7, no. 6, pp. 693–701, Jul. 2013.
[4] H. Cheng, L. Xiaorui, L. Teng, and G. Yangte, "GEO SAR interferometry: Theory and feasibility study," in *Proc. Radar Conf., IET*, Apr. 14–16, 2013, pp. 1–5.
[5] Z. Qingjun, G. Yangte, G. Wenjun, L. Jiaoshan, and L. Ke, "3D orbit selection for regional observation GEO SAR," *Neurocomput.*, vol. 151, no. 2, pp. 692–699, Mar. 2015.
[6] C. Prati, F. Rocca, D. Giancola, and A. Monti Guarnieri, "Passive geosynchronous SAR system reusing backscattered digital audio broadcasting signals," *IEEE Trans. Geosci. Remote Sens.*, vol. 36, no. 6, pp. 1973–1976, Nov. 1998.
[7] J. Ruiz-Rodon, A. Broquetas, E. Makhoul, A. Monti Guarnieri, and F. Rocca, "Nearly zero inclination geosynchronous SAR mission analysis with long integration time for Earth observation," *IEEE Trans. Geosci. Remote Sens.*, vol. 52, no. 10, pp. 6379–6391, Oct. 2014.
[8] G. Wadge, A. Monti Guarnieri, S. E. Hobbs, and D. Schultz, "Potential atmospheric and terrestrial applications of a geosynchronous RADAR," in *Proc. IGARSS*, Jul. 13–18, 2014, pp. 946–949.
[9] L. Iannini and A. Monti Guarnieri, "Atmospheric phase screen in ground-based radar: Statistics and compensation," *IEEE Geosci. Remote Sens. Lett.*, vol. 8, no. 3, pp. 537-541, May 2011.
[10] D. Bruno and S. E. Hobbs, "Radar imaging from geosynchronous orbit: Temporal decorrelation aspects," *IEEE Trans. Geosci. Remote Sens.*, vol. 48, no. 7, pp. 2924–2929, Jul. 2010.
[11] A. Recchia, A. Monti Guarnieri, A. Broquetas, and J. Ruiz-Rodon, "Assessment of atmospheric phase screen impact on geosynchronous SAR," in *Proc. IGARSS*, Jul. 13–18, 2014, pp. 2253–2256.
[12] D. Massonnet, "Capabilities and limitations of the interferometric cartwheel," *IEEE Trans. Geosci. Remote Sens.*, vol. 39, no. 3, pp. 506–520, Mar. 2001.
[13] G. Krieger, "MIMO-SAR: Opportunities and pitfalls," *IEEE Trans. Geosci. Remote Sens.*, vol. 52, no. 5, pp. 2628–2645, May 2014.
[14] D. Cristallini, D. Pastina, and P. Lombardo, "Exploiting MIMO SAR potentialities with efficient cross-track constellation configurations for improved range resolution," *IEEE Trans. Geosci. Remote Sens.*, vol. 49, no. 1, pp. 38-52, Jan. 2011.
[15] L. Cazzani *et al.*, "A ground-based parasitic SAR experiment," *IEEE Trans. Geosci. Remote Sens.*, vol. 38, no. 5, pp. 2132–2141, Sep. 2000.
[16] S. Tebaldini, F. Rocca, and A. Monti Guarnieri, "Model based SAR tomography of forested areas," in *Proc. IGARSS*, Jul. 7–11, 2008, vol. 2, pp. 593–596.
[17] P. Wauthier, P. Francken, and H. Laroche, "Co-location of six ASTRA satellites: Assessment after one year of operations," in *Proc. 12th Int. Symp. Space Flight Dynam.*, Aug. 1997, pp. 13–18.
[18] A. Moccia and A. Renga, "Synthetic aperture radar for Earth observation from a lunar base: Performance and potential applications," *IEEE Trans. Aerosp. Electron. Syst.*, vol. 46, no. 3, pp. 1034–1051, Jul. 2010.
[19] G. Fornaro, G. Franceschetti, F. Lombardini, A. Mori, and M. Calamia, "Potentials and Limitations of Moon-Borne SAR Imaging," *IEEE Trans. Geosci. Remote Sens.*, vol. 48, no. 7, pp. 3009–3019, Jul. 2010.